Award Number G10AP00037

John E. Ebel, Anastasia Moulis and Jake J. Martin

Weston Observatory
Department of Geology and Geophysics
Boston College
Weston, MA 02493
(617) 552-8300
Fax: (617) 552-8388

Principal Investigator: John E. Ebel
ebel@bc.edu

Project Duration: January 1, 2010 to December 31, 2010

Award Title: ANALYSIS OF AFTERSHOCK SEQUENCES FOR USE IN PREDICTING AFTERSHOCK PROBABILITIES IMMEDIATELY FOLLOWING STRONG EARTHQUAKES

Final Report

Submitted
March, 2011

"Research supported by the U.S. Geological Survey (USGS), Department of the Interior, under USGS award number G10AP00037. The views and conclusions contained in this document are those of the authors and should not be interpreted as necessarily representing the official policies, either expressed or implied, of the U.S. Government."

ANALYSIS OF AFTERSHOCK SEQUENCES FOR USE IN PREDICTING AFTERSHOCK PROBABILITIES IMMEDIATELY FOLLOWING STRONG EARTHQUAKES

Award Number G10AP00037

John E. Ebel, Anastasia Moulis and Jake J. Martin

Weston Observatory
Department of Geology and Geophysics
Boston College
Weston, MA 02493
(617) 552-8300
Fax: (617) 552-8388

Principal Investigator: John E. Ebel
ebel@bc.edu

Project Duration: January 1, 2010 to December 31, 2010

Abstract

The goal of this research project was to seek ways to improve the accuracy of aftershock forecasts issued within 1-2 hours of a strong crustal earthquake anywhere in the U.S. A dataset of 61 earthquakes with M≥5.0 in California from 1971 to 2009 was analyzed. The aftershock sequences were described using the Reasenberg and Jones (1989) version of Omori's law, for which three parameters are determined: *b*, which is the b value from the Gutenberg-Richter recurrence relation for the aftershock sequence; *p*, which is the exponent of the Omori's Law temporal decay; and *a*, which is a constant based on the aftershock activity rate at t=0.95. Correlations of the *a*, *b* and *p* parameters with hypocentral depth, stress drop, focal mechanism, and surface faulting were investigated. The most robust statistical result is that on average thrust earthquakes generate more prodigious aftershock sequences than strike-slip earthquakes. The presence or absence of surface rupture may exert some control on the average Omori-Law parameters of aftershock patterns, but the effect is not very statistically significant. There is no correlation between any of the Omori-Law parameters and hypocentral depth or stress drop. No seasonal pattern is seen for any of the Omori-Law parameters, which suggests that rainfall does not play a controlling the generation of aftershock activity following a strong earthquake. The depth range where most aftershocks take place seems to be more controlled by where in California the mainshock takes place than by the focal mechanism or the presence or absence of surface faulting of the mainshock. The analyses detailed in this report suggest that source parameters that are available within an hour or two of a strong mainshock in California provide very little indication of what kind of aftershock sequence will follow the mainshock.

Introduction

The goal of this research project was to seek ways to improve the accuracy of aftershock forecasts issued within 1-2 hours of a strong crustal earthquake anywhere in the U.S. While forecasting future mainshocks is a very uncertain process for which there is no proven method at the present time, statistical forecasts of the probabilities of future aftershocks after a large earthquake is, in theory, possible with some reliability (e.g., Reasenberg and Jones, 1989). Unfortunately, there is a wide range in the behavior of earthquake aftershock sequences from one mainshock to another. Some earthquakes are profuse in the number of aftershocks that they generate, while other earthquakes are relatively aftershock-poor. Some mainshocks are followed by strong aftershocks, while others are not. This wide range in aftershock activity causes large uncertainties in the initial aftershock forecasts that are issued immediately following the occurrence of a strong earthquake. This is unfortunate because the greatest aftershock hazard occurs in the first 24-48 hours after a mainshock. The time of greatest uncertainty in forecasting expected aftershock rates coincides with the time when search-and-rescue efforts must take place if the mainshock was damaging to local population centers. Clearly, improving the accuracy of aftershock forecasts issued within 1-2 hours of a strong earthquake is an important goal that can help save lives and prevent injuries.

At the present time there is a paucity of investigations into why some earthquakes generate a large number of aftershocks and other earthquakes do not. The rate-and-state theory developed by Dieterich (1994) predicts that the average rate of aftershock decay is a function of the mainshock recurrence time and of the stressing history. However, for most faults the mainshock recurrence times and stress histories are not well known, and so testing Dieterich's ideas with observational data from real earthquakes is still quite difficult. Do rates of aftershock activity depend on the stress drop of the mainshock? Do they depend on the local deformation rate as measured geodetically? Is there a dependence of aftershock generation on focal depth for earthquakes that are confined to the crust? The research described in this report addresses these questions about possible factors that may control the generation of aftershocks using dataset of aftershock sequences of M≥5.0 earthquakes from California.

Aftershock Data Set

A dataset of 61 earthquakes with M≥5.0 in California from 1971 to 2009 was selected as the database for this study (Table 1). The earthquake dataset was confined to California because there is a long history of dense earthquake monitoring in the state, meaning that there is almost 40 years of well-recorded aftershock sequences within the state. Reasenberg and Jones (1989) have already determined the Omori-Law parameters for a number of aftershock sequences in California, and they made their dataset available to us for this study (L. Jones, 2010). For each earthquake in Table 1 for which no Omori-Law parameters were in the Reasenberg and Jones dataset, aftershocks were extracted from either the Northern California Data Center or the Southern California Data Center, and these extracted aftershocks were analyzed for their Omori-Law parameters. In

addition, a literature search was carried out to find source parameters such as focal mechanism, stress drop, rupture area, and directivity for as many of the earthquakes in Table 1 as possible. Table 2 lists those literature references from which the source parameters for the earthquakes in Table 1 were taken.

The parameterization of Omori's Law that was used in this study is that of Reasenberg and Jones (1989). Their formulation of Omori's Law gives the relationship for the activity rate λ at or above magnitude M at time t after a mainshock as

$$log10(\lambda(t,M)) = a + b(Mm-M) - p\ log10(t + 0.05) \qquad (1)$$

where Mm is the mainshock magnitude, b is the b value from the Gutenberg-Richter recurrence relation for the aftershock sequence, p is the exponent of the Omori's Law temporal decay, a is a constant based on the aftershock activity rate at t=0.95, and M is the minimum magnitude for which the aftershock rate is being computed. Note that the a parameter in Equation (1) is somewhat different from a in the standard Gutenberg-Richter relation.

Also shown in Table 1 is a column labeled *N1* is another way to describe the aftershock activity of a mainshock. *N1* is the number of aftershocks of M≥2.0 that are computed for the first day after the mainshock, as calculated using the Omori-Law parameters a, b and p for that aftershock sequence.

The parameters a, b and p in Table 1 were investigated to see if there are any mutual dependencies among those parameters. While they are distinct parameters in Equation (1), it is possible that that these parameters might not be independent in observed aftershock sequences. Figure 1 shows correlation plots of a, b and p. In Figure 1 it can be seen that the parameter p does not correlate with either a or b, but that there is some inverse correlation of a and b. Thus, for the observed aftershock sequences analyzed in this study, a and b are not totally independent of each other.

Analyses of Aftershock Parameters

A number of analyses were carried out to look for correlations of the Omori-Law aftershock parameters of Table 1 with commonly reported source parameters of mainshocks, especially those source parameters that can be determined within a short period of time (minutes to a couple of hours) of the occurrence of a mainshock. The goal of this work is to look for those parameters (or combinations of parameters) that may indicate which mainshocks will have more active aftershock sequences and which will have less active aftershock sequences. In this study, this analysis is carried out by looking for correlations of the a, b and p parameters with a number of different mainshock parameters.

Correlation with Focal Depth

One correlation that was carried out was of the Omori-Law parameters and focal depth (Figure 2). It is well known that earthquakes with deeper hypocenters (deeper than about 50 km) have much less active aftershock sequences than earthquakes with shallower hypocenters. This analysis looks to see if there is depth dependence of any of the Omori-Law parameters with focal depth for the crustal earthquakes in California. In Figure 2, no clear focal depth dependence is seen for any of the Omori-Law parameters. Visually, there appears to be a slight decrease in *b* value with focal depth, but this is not statistically significant.

Correlation with Stress Drop

Another correlation that was carried out was of the Omori-Law parameters and static stress drop (Figure 3). The stress drops in Figure 3 were compiled from a list of stress-drop determination provided by Robert Darragh of Pacific Engineering and Analysis. Only a subset of the earthquakes in Table 1 have stress drop determinations in the Darragh dataset. In Figure 3, no clear stress-drop dependence is seen for any of the Omori-Law parameters.

The static stress-drop values in Figure 3 from R. Darragh were all determined using a common method. A literature search for published static stress drops revealed that stress-drop values found by different investigators for the same earthquakes are significantly different than those used in Figure 3. This reflects the different methods that are used to make static stress-drop estimates as well as uncertainties in the input parameters for stress-drop calculations. For example, for the 1987 M 6.6 Superstition Hills earthquake in Southern California, Darragh reports a static stress drop of .41 MPa. Moghaddam et al. (2010) report three different static stress-drop values for this earthquake using three different methods: 4.8 MPa (PEER-NGA determination), 9.5 MPa (based on point-source modeling) and 8.5 MPa (based on finite fault modeling). Mohammadioun and Serva (2001) report a stress drop of 1.0 MPa for this event. Estimates of the static stress drop for this single earthquake from different investigators vary by more than one order of magnitude. Thus, the lack of correlation of any of the Omori-Law parameters with static stress drop may reflect large uncertainties in the static stress-drop determinations.

Correlation with Time of Year

California has a strongly seasonal rainfall pattern, with virtually all of its rainfall occurring in the fall, winter or early spring. Little or no rainfall is experienced in the state during the late spring, summer and early fall. Variations in the water contained in faults and underground pores can influence seismicity (Costain et al., 1987), and so it might be expected that seismicity parameters would show a seasonal variation. This analysis looks for seasonal variations in the Omori-Law parameters that would reflect a response of aftershocks to the seasonal variations in the groundwater that is contained in fault zones.

Figure 4 shows the monthly values of *a*, *b* and *p* for the dataset of Table 1. The data are plotted versus the month of the mainshock in Figure 4, and the primary aftershock activity following each mainshock can extend into one or two months following the mainshock. No seasonal pattern is seen in Figure 4 for any of the Omori-Law parameters, which suggests that rainfall does not play a controlling role in the generation of aftershock activity following a strong earthquake.

Correlation with Focal Mechanism

Most strong earthquakes in California have strike-slip focal mechanisms on vertical or near-vertical faults, and almost all of the rest of the strong earthquakes have thrust focal mechanisms or oblique focal mechanisms with combined thrust and strike-slip components. For the correlation analysis in this study, the focal mechanisms of the earthquakes in Table 1 were divided into two classes. For each earthquake, the fault plane of the event was determined from surface faulting, the spatial locations of its aftershocks, or from the predominant orientation of the active faults in the vicinity of the event. Focal mechanisms with rakes between -45° (+315°) and +45° or between +135° and +225° were classified as strike-slip earthquakes. The remaining events were classified as thrust earthquakes if their rake is between +45° and +135° and as normal earthquakes if their rake is between +225° and +315° (-45°). The thrust and normal earthquakes were lumped into a single classification denoted "not strike-slip" in this study. In most cases, the rake of an earthquake put it unquestionably into the strike-slip or the not strike-slip classification. Searches of the literature and of the internet were carried out to find the focal mechanism of each mainshock in this study.

Figure 5 displays the distributions of the *a*, *b* and *p* parameters for the strike-slip and not strike-slip classes of earthquakes. Also shown in Figure 5 is the mean value of each of the Omori-Law parameters for each earthquake classification. The mean values of the *p* values for the two earthquake classifications are equal, and the mean values for the two earthquake classifications are close to each other for the *b* values. On the other hand, the mean *a* value for the strike-slip earthquakes is much more negative than that for the not strike-slip earthquakes. The difference in the mean *a* values of the strike-slip and not strike-slip earthquakes is statistically significant at the 95% confidence level. For a given *b* value, an aftershock sequence with a less negative value of *a* has a higher rate of activity than an aftershock sequence with a more negative value of *a*. This analysis indicates that on average strike-slip mainshocks generate less active aftershock sequences than mainshocks with a strong thrust or normal component of slip.

Correlation with Surface Faulting

Many strong earthquakes in California are associated with surface faulting, primarily those with strike-slip focal mechanisms. An analysis was carried out to see if there is any systematic difference in the Omori-Law parameters for those earthquakes that had surface faulting and those earthquakes for which no surface faulting was

observed. The results of this analysis are shown in Figure 6. The earthquake data used in Figure 6 exclude events from the Cape Mendocino area, because many of the earthquakes in that area had offshore ruptures for which the presence or absence of surface faulting could not be determined.

The distributions of the *a*, *b* and *p* parameters for earthquakes with and without surface faulting show some differences in Figure 6. Specifically, earthquakes with no surface faulting tend to have a higher *b* value, a lower *p* value and a lower *a* value on average than those earthquakes for which surface faulting was observed. On the other hand, none of these differences is significant at the 95% confidence interval, and only the difference in the mean *b* values is significant at the 90% confidence interval.

Depth Distributions of Aftershocks

One other analysis that was carried out was to examine the depth distributions of a number of well-recorded aftershock sequences that followed large mainshocks. The goal of this analysis was to see if aftershock depth distributions are controlled by the focal mechanism of the mainshock or by the presence or absence of surface faulting. Figure 7 shows box plots of the depth distributions of 12 well-recorded aftershock sequences. Curiously, in Figure 7 it can be seen that the presence or absence of surface faulting does not control the depth range where the majority of the aftershocks take place following a mainshock. Most of the aftershocks of the 1979 Imperial Valley earthquake and the 2004 Parkfield earthquake were below 5 km, even though both of these earthquakes had surface faulting. On the other hand, the Joshua Tree and Big Bear earthquakes both had most of their aftershocks at depths of about 5 km or less, even though no surface faulting was found for either event. Perhaps the most systematic pattern that can be discerned in Figure 7 is that the predominant aftershock depth range appears to be a function of where in California the mainshock takes place. The earthquakes in the Mojave Desert (Joshua Tree, Big Bear, Landers and Hector Mine) all have aftershock sequences that take place primarily within 6 km of the earth's surface. On the other hand, the three earthquake sequences from central California (San Simeon, Loma Prieta and Coalinga) had aftershocks sequences that were primarily between about 4 km and 12 km depth. The 1971 San Fernando earthquake and the 1994 Northridge earthquake, both thrust events that are approximately on conjugate fault planes, have very similar aftershock depth distributions. Curiously, the 1979 Imperial Valley earthquake, which ruptured to the surface, had most of its aftershocks take place at focal depths greater than about 8 km. Surface rupture appears to be a surprisingly poor indicator of the depth range where most aftershocks take place.

Discussion and Conclusions

The analyses detailed in the previous subsections of this report suggest that source parameters that are available with an hour or two of a strong mainshock in California provide very little indication of what kind of aftershock sequence will follow the mainshock. The most robust statistical result is that thrust earthquakes generate more

prodigious aftershock sequences than strike-slip earthquakes. The presence or absence of surface rupture may exert some control on the average Omori-Law parameters of the aftershock patterns, but the effect is not very statistically significant. The depth range where most of the aftershocks take place seems to be more controlled by where in California the mainshock was centered than by the focal mechanism or the presence or absence of surface faulting of the mainshock. Thus, the forecasting of aftershock activity immediately following a mainshock remains a rather uncertain enterprise.

Acknowledgments

Lucy Jones is thanked for providing the Omori-Law parameters for many of the earthquakes analyzed in this study. Bob Darragh is thanks for providing his dataset of static stress drops for California earthquakes.

References

Costain, J.K., G.A. Bollinger and J.K. Speer (1987). Hydroseismicity; a hypothesis for the role of water in the generation of intraplate seismicity, *Seism. Res. Lett.* **15**, 618-621.

Dieterich, J. (1994). A constitutive law for rate of earthquake production and its application to earthquake clustering, *J. Geophys. Res.* **99**, 2601-2618.

Moghaddam, H., N. Fanaie, and D. Motazedian (2010). Estimation of Stress Drop for Some Large Shallow Earthquakes Using Stochastic Point Source and Finite Fault Modeling, *Trans. A: Civil Eng.*, **17**, 217-235.

Mohammadioun, B. and L. Serva (2001). Stress Drop, Slip Type, Earthquake Magnitude, and Seismic Hazard, *Bull. Seism. Soc. Am.* **91**, 694-707.

Reasenberg, P.A. and L.M. Jones (1989). Earthquake Hazard After a Mainshock in California, *Science* **243**, 1173-1176.

Publications Based on This Research

Ebel, J.E., and J.J. Martin (2010). Factors Controlling Aftershock Activity after M≥ 5 Earthquakes in California, Abstract S42B-03. presented at 2010 Fall Meeting, AGU, San Francisco, Calif., 13-17 Dec.

Table 1. Study Earthquakes

Date	Origin Time (hr:min)	Magnitude	Latitude (°N)	Longitude (°E)	Depth (km)	b	p	a	N1
2/9/71	14:00	6.6	34.411	-118.401	8.4	1.040	1.240	-2.060	530
2/24/72	15:56	5.0	36.578	-121.209	6.5	1.010	0.790	-1.700	21
2/21/73	14:45	5.5	34.065	-119.035	17.0	0.570	0.750	-1.320	5
11/28/74	23:01	5.2	36.916	-121.478	6.0	0.940	0.790	-2.270	5
6/1/75	1:38	5.2	34.516	-116.496	5.8	1.000	1.070	-2.150	11
8/1/75	20:20	5.7	39.436	-121.523	5.5	0.590	0.930	-0.780	25
1/10/76	12:58	5.0	32.084	-115.471	12.0	0.810	0.560	-1.400	11
5/5/78	21:03	5.2	32.211	-115.304	10.0	1.060	0.820	-2.450	9
8/13/78	22:54	5.1	34.347	-119.696	12.7	1.200	1.120	-2.220	32
10/4/78	16:42	5.8	37.514	-118.683	16.0	0.800	1.380	-1.440	40
1/1/79	23:14	5.0	33.944	-118.681	11.3	0.870	1.170	-1.330	19
3/15/79	21:07	5.2	34.327	-116.445	9.3	0.990	1.010	-1.390	60
8/6/79	17:05	5.9	37.110	-121.511	6.3	0.950	1.040	-2.550	14
10/15/79	23:16	6.6	32.614	-115.318	12.0	1.000	1.490	-2.010	389
1/24/80	19:00	5.9	37.826	-121.786	11.0	0.900	1.080	-2.170	22
2/25/80	10:47	5.5	33.001	-116.513	19.4	0.950	1.100	-2.390	9
9/7/80	4:37	5.7	37.994	-118.402	10.5	0.900	0.960	-1.670	46
4/26/81	12:09	5.7	33.099	-115.632	18.8	0.990	1.340	-2.070	39
9/4/81	15:50	5.3	33.671	-119.111	11.5	0.770	0.900	-1.460	12
10/25/82	22:26	5.4	36.319	-120.516	11.9	0.790	0.950	-1.830	7
1/7/83	1:38	5.7	37.656	-118.929	7.0	0.890	1.080	-1.190	127
1/23/84	5:40	5.2	36.353	-121.909	7.2	0.500	1.320	-1.220	2
4/24/84	21:15	6.2	37.314	-121.657	8.0	1.010	0.870	-3.250	10
5/28/84	14:50	6.2	37.503	-118.806	14.8	1.179	0.732	-3.772	15

6/10/84	3:28	6.3	32.200	-115.122	9.0	1.096	1.206	-2.479	172
11/9/84	10:27	7.2	41.084	-124.616	19.0	0.953	1.176	-3.675	19
11/23/84	18:08	6.2	37.470	-118.597	9.2	0.960	1.080	-1.710	210
8/4/85	12:01	5.8	36.151	-120.049	11.0	1.040	0.940	-2.410	35
1/26/86	19:20	5.7	36.809	-121.288	8.4	1.100	1.080	-2.930	14
3/31/86	11:55	5.7	37.467	-121.692	8.0	1.150	0.910	-3.140	13
7/13/86	9:20	5.9	33.999	-116.609	10.4	0.930	1.170	-1.590	109
7/13/86	13:47	5.5	32.972	-117.873	6.0	1.340	0.750	-2.580	129
7/21/86	14:42	6.5	37.543	-118.444	6.0	0.920	1.190	-1.770	234
2/7/87	3:45	5.4	32.393	-115.311	5.6	0.670	1.510	-1.410	19
5/3/87	23:42	6.7	36.232	-120.312	10.0	1.200	1.300	-2.600	30
7/31/87	23:56	5.5	40.409	-124.407	7.4	0.930	1.046	-1.345	1057
10/1/87	14:42	6.0	34.061	-118.079	9.5	1.020	1.200	-2.300	19
6/10/88	23:06	5.4	34.943	-118.743	6.8	1.190	1.440	-3.530	1
9/11/88	3:14	6.6	40.504	-125.130	10.0	1.070	1.220	-2.900	5
12/3/88	11:38	4.9	34.141	-118.133	13.3	0.940	0.511	-4.123	2
11/25/91	1:54	6.2	33.090	-115.792	10.6	0.847	1.265	-1.798	57
11/25/91	13:15	6.6	33.015	-115.852	2.0	1.096	1.290	-2.937	127
10/19/93	0:04	7.0	37.036	-121.880	11.0	0.923	0.936	-1.954	456
7/14/95	2:50	6.6	42.019	-125.717	11.0	1.056	1.189	-4.665	2
8/17/95	22:26	6.1	41.661	-125.846	12.0	1.084	1.140	-3.425	10
8/18/95	19:29	6.0	40.252	-124.286	12.0	0.932	0.983	-2.552	15
8/18/95	22:17	6.5	41.679	-125.856	14.0	1.176	0.996	-4.465	7
4/24/96	4:50	6.1	33.960	-116.317	11.4	1.079	0.840	-2.922	32
4/26/96	18:06	6.7	40.335	-124.229	15.0	0.859	0.795	-1.388	439
4/27/96	7:41	6.5	40.433	-124.566	20.0	0.970	0.946	-2.045	187
4/27/96	11:18	6.6	40.383	-124.555	22.0	0.970	0.946	-2.045	244
6/29/96	11:57	7.3	34.200	-116.437	5.0	1.032	1.091	-3.037	270

6/29/96	15:05	6.3	34.203	-116.827	5.0	0.992	1.062	-2.433	68
5/18/97	23:20	6.4	37.166	-117.780	13.0	0.741	1.196	-0.476	569
1/18/98	12:30	6.7	34.213	-118.537	16.0	0.830	1.090	-1.314	388
9/2/98	15:15	7.0	40.406	-125.680	10.0	0.772	0.715	-2.522	22
2/20/99	4:03	6.6	40.592	-125.757	10.0	0.939	0.872	-3.563	6
10/17/03	9:46	7.1	34.594	-116.271	5.0	0.980	1.092	-2.631	233
12/23/07	19:15	6.5	35.701	-121.101	7.6	1.364	0.922	-4.658	30
6/16/09	2:50	7.0	41.233	-125.986	16.0	0.950	0.996	-4.155	4
6/18/09	6:21	6.5	40.646	-126.358	12.0	0.755	1.218	-2.063	20

Table 2. Literature sources used for the data shown in Figures 2-7.

Anderson, J.G. (1984). The 4 September 1981 Santa Barbara Island, California, earthquake: Interpretation of strong motion data, *Bull. Seism. Soc. Am.* **74**, 995-1010.

Boatwright, J., and D.M. Boore (1982). Analysis of the ground accelerations radiated by the 1980 Livermore Valley earthquakes for directivity and dynamic source characteristics, *Bull. Seism. Soc. Am.* **72**, 1843-1865.

Boore, D.M., and D.J. Stierman (1976). Source parameters of the Pt. Mugu, California, earthquake of February 21, 1973, *Bull. Seism. Soc. Am.* **66**, 385-404.

Boore, D.M., W.B. Joyner and T.E. Fumal (1997). Equations for estimating horizontal response spectra and peak acceleration from western North American earthquakes; a summary of recent work, *Seism. Res. Lett.* **68**, 128-153.

Corbett, E.J., and C.E. Johnson (1982). The Santa Barbara, California, earthquake of 13 August 1978, *Bull. Seism. Soc. Am.* **72**, 2201-2226.

Dengler, L. and R. McPherson (1993). The 17 August 1991 Honeydew earthquake, North Coast California: A case for revising the Modified Mercalli scale in sparsely populated areas, *Bull. Seism. Soc. Am.* **83**, 1081-1094.

Ekstrom, G., R.S. Stein, J.P. Eaton and D. Eberhart-Phillips (1992). Seismicity and geometry of a 110-km-long blind thrust fault; 1, The 1985 Kettleman Hills, California, earthquake, *J. Geophys. Res.* **97**, 4843-4864.

Ellsworth, W.L. (1975). Bear Valley, California, earthquake sequence of February-March 1972, *Bull. Seism. Soc. Am.* **65**, 483-506.

Given, J.W., T.C. Wallace and H. Kanamori (1982). Teleseismic analysis of the 1980 Mammoth Lakes earthquake sequence, *Bull. Seism. Soc. Am.* **72**, 1093-1109.

Glowacka, E., and F.A. Nava (1996). Major earthquakes in Mexicali Valley, Mexico, and fluid extraction at Cerro Prieto Geothermal Field, *Bull. Seism. Soc. Am*. **86**, 93-105.

Hardebeck, J.L., J. Boatwright, D. Dreger, R. Goel, V. Graizer, K. Hudnut, C. Ji., L. Jones, J. Langbein, J. Lin, E. Roeloffs, R. Simpson, K. Stark, R. Stein and J.C. Tinsley (2004). Preliminary report on the 22 December 2003, M 6.5 San Simeon, California earthquake, *Seism. Res. Lett.* **75**, 155-172.

Hartzell, S., and J.N. Brune (1979). The horse canyon earthquake of August 2, 1975—Two-stage stress-release process in a strike-slip earthquake, *Bull. Seism. Soc. Am.* **69**, 1161-1173.

Hartzell, S.H., and T.H. Heaton (1983). Inversion of strong ground motion and teleseismic waveform data for the fault rupture history of the 1979 Imperial Valley, California, earthquake, *Bull. Seism. Soc. Am.* **73**, 1553-1583.

Hauksson, E. and J.W. Saldivar (1986). The 1930 Santa Monica and the 1979 Malibu, California, earthquakes, *Bull. Seism. Soc. Am.* **76**, 1542-1559.

Hough, S.E., and D.S. Dreger (1995). Source parameters of the 23 April 1992 M 6.1 Joshua Tree, California, earthquake and its aftershocks: Empirical Green's function analysis of GEOS and TERRAscope data, *Bull. Seism. Soc. Am.* **85**, 1576-1590.

Huang, L.J., H. Magistrale and H. Kanamori (1990). Teleseismic source parameters and rupture characteristics of the 24 November 1987, Superstition Hills earthquake, *Bull. Seism. Soc. Am*. **80**, 43-56.

Hudnut, K., L. Seeber, T. Rockwell, J. Goodmacher, R. Klinger, S. Lindvall and R. McElwain (1989). Surface ruptures on cross-faults in the 24 November 1987 Superstition Hills, California, earthquake sequence, *Bull. Seism. Soc. Am.* **79**, 282-296.

Jones, L.E. and S.E. Hough (1995). Analysis of broadband records from the 28 June 1992 Big Bear earthquake: Evidence of a multiple-event source, *Bull. Seism. Soc. Am.* **85**, 688-704.

Kanamori, H. and G. Fuis (1976). Variation of P-wave velocity before and after the Galway Lake earthquake (ML = 5.2) and the Goat Mountain earthquakes (ML = 4.7, 4.7), 1975, in the Mojave Desert, California, *Bull. Seism. Soc. Am.* **76**, 2017-2037.

Kanamori, H. and J.W. Given (1982). Use of long-period surface waves for rapid determination of earthquake source parameters; II, Preliminary determination of source mechanisms of large earthquakes (M s > or =6.5) in 1980, *Phys. Earth Planet. Int.* **30**, 260-268.

Kanamori, H., and C.R. Allen (1986). Earthquake repeat time and average stress drop, *Earthquake Source Mechanics*, Geophysical Monograph **37**, 227-235.

Kanamori, H., J. Mori and T.H. Heaton (1990). The 3 December 1988, Pasadena earthquake (ML = 4.9) recorded with the very broadband system in Pasadena, *Bull. Seism. Soc. Am.* **80**, 483-487.

Kanamori, H., H.K. Thio, D.S. Dreger, E. Hauksson and T. Heaton (1992). Initial investigation of the Landers, California, earthquake of 28 June 1992 using TERRAscope, *Geophys. Res. Lett.* **19**, 2267-2270.

King, G.C.P., R.S. Stein and J. Lin (1994). Static stress changes and the triggering of earthquakes, *Bull. Seism. Soc. Am.* **84**, 935-953.

Lin J. and R.S. Stein (1989). Coseismic folding, earthquake recurrence, and the 1987 source mechanism at Whittier Narrows, Los Angeles Basin, California, *J. Geophys. Res.* **94**, 9614-9632.

Mayeda, K., and W.R. Walter (1996). Moment, energy, stress drop, and source spectra of Western United States earthquakes from regional coda envelopes, *J. Geophys. Res.* **101**, 11,195-11,208.

McGill, S.F., C.R. Allen, K.R. Hudnut, D.C. Johnston, W.F. Miller and K.F. Sieh (1989). Slip on the Superstition Hills fault and on nearby faults associated with the 24 November 1987 Elmore Ranch and Superstition Hills earthquakes, Southern California, *Bull. Seism. Soc. Am.* **79**, 362-375.

Mikumo, T. and T. Miyataki (1995). Heterogeneous distribution of dynamic stress drop and relative fault strength recovered from the results of waveform inversion: the 1984 Morgan Hill, California, earthquake, *Bull. Seism. Soc. Am.* **85**, 178-193.

Pacheco, J. and J. Nabelek (1988). Source mechanisms of three moderate California earthquakes of July 1986, *Bull. Seism. Soc. Am*. **78**, 1907-1929.

Peppin, W.H., W. Honjas, M.R. Somerville and U.R. Vetter (1989). Precise master-event locations of aftershocks of the 4 October 1978 Wheeler Crest earthquake sequence near Long Valley, California, *Bull. Seism. Soc. Am.* **79**, 67-76.

Quin, H., (1990). Dynamic stress drop and rupture dynamics of the October 15, 1979 Imperial Valley, California, earthquake, *Tectonophysics* **175**, 93-117.

Rabinovich, A.B., F.E. Stephenson and R.E. Thomson (2006). The California Tsunami of 15 June 2005 along the Coast of North America, *Atmosphere-Ocean* **44**, 415-427.

Sharp, R.V., M.J. Rymer and J.J. Lienkaemper (1986). Surface displacement on the Imperial and Superstition Hills faults triggered by the Westmorland, California, earthquake of 26 April 1981, *Bull. Seism. Soc. Am.* **76**, 949-965.

Stein, R.S., and M. Liskowski (1983). The 1979 Homestead Valley earthquake sequence, California; control of aftershocks and postseismic deformation, *J. Geophys. Res.* **88**, 6477-6490.

Toda, S., and R.S. Stein (2002). Response of the San Andreas fault to the 1983 Coalinga-Nuñez earthquakes: An application of interaction-based probabilities for Parkfield, *J. Geophys. Res*. 107, DOI 10.1029/2001JB000172.

Trifunac, M.D. (1972). Stress estimates for the San Fernando, California, earthquake of February 9, 1971: Main event and thirteen aftershocks, *Bull. Seism. Soc. Am.* **62**, 721-750.

Trifunac, M.D. (1974). A three-dimensional dislocation model for the San Fernando, California, earthquake of February 9, 1971, *Bull. Seism. Soc. Am.* **64**, 149-172.

Trifunac, M.D., and F.E. Udwadia (1974). Parkfield, California, earthquake of June 27, 1966: A three-dimensional moving dislocation, *Bull. Seism. Soc. Am.* **64**, 511-533.

Urhammer, R.A. (1980) Observations of the Coyote Lake, California earthquake sequence of August 6, 1979, *Bull. Seism. Soc. Am.* **70**, 559-570.

Velasco, A.A., C.J. Ammon and T. Lay (1994). Recent large earthquakes near Cape Mendocino and in the Gorda Plate; broadband source time functions, fault orientations, and rupture complexities, *J. Geophys. Res.* **99**, 711-728.

Wald D.J., D.V. Helmberger and T.H. Heaton (1991). Rupture model of the 1989 Loma Prieta earthquake from the inversion of strong-motion and broadband teleseismic data, *Bull. Seism. Soc. Am.* **81**, 1540-1572.

Wald, D.J., D.V. Helmberger and S.H. Hartzell (1990). Rupture process of the 1987 Superstition Hills earthquake from the inversion of strong-motion data, *Bull. Seism. Soc. Am.* **80**, 1079-1098.

Wong, V., J. Frez and F. Suarez (1997). The Victoria, Mexico, earthquake of June 9, 1980, *Geofisica Internacional* **36**, 139-159.

Zhou Y., C. McNally and T. Lay (1993). Analysis of the 1986 Mt. Lewis, California, earthquake; preshock sequence-mainshock-aftershock sequence, *Phys. Earth Planet. Int.* **75**, 267-288.

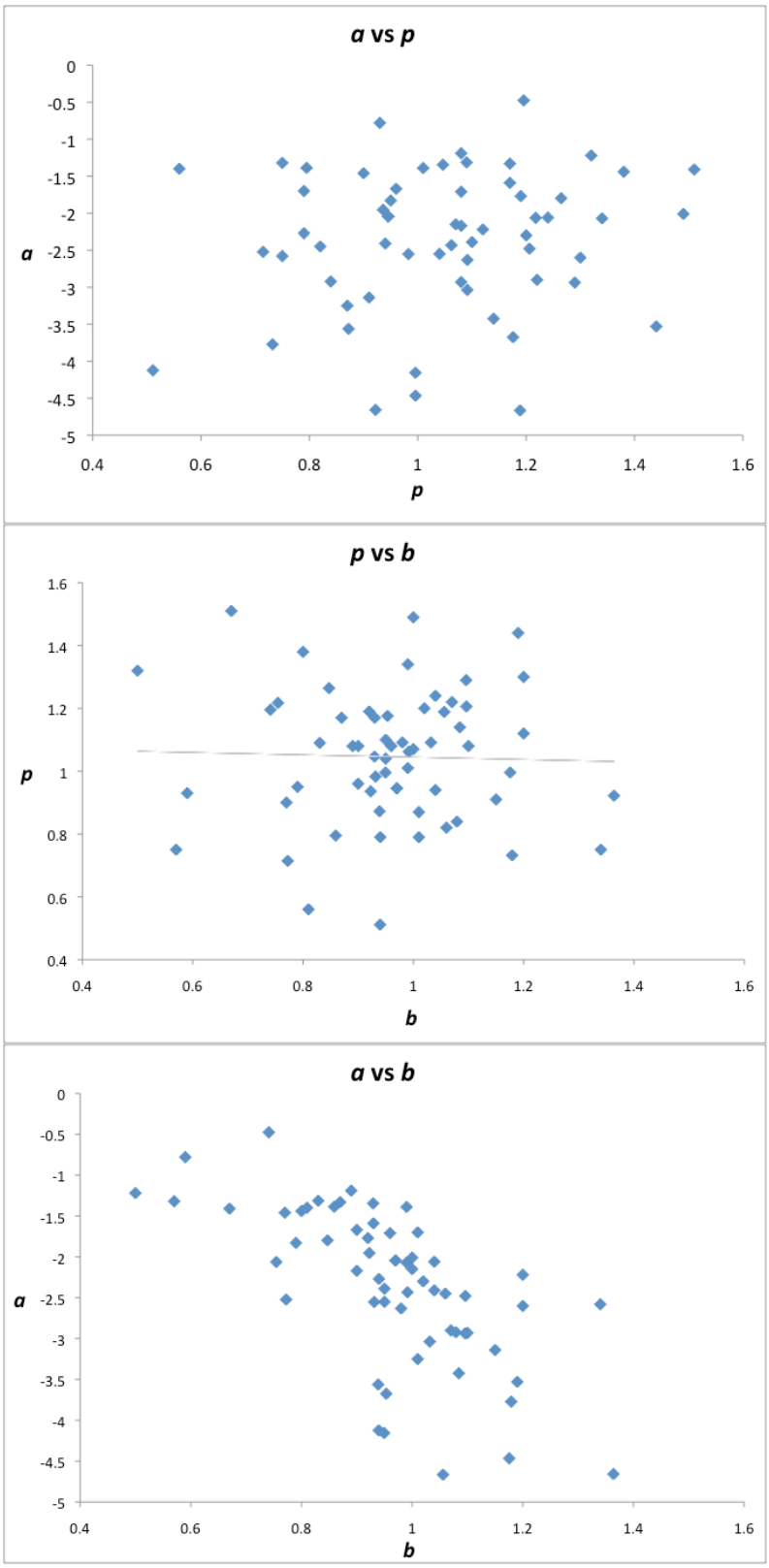

Figure 1. Correlations of the Omori-Law parameters (top) *a* with *p*, (middle) *p* with *b*, and (bottom) *a* with *b*. There is no correlation of the parameter *p* with *a* or *b*, but *a* and *b* show evidence of an inverse correlation.

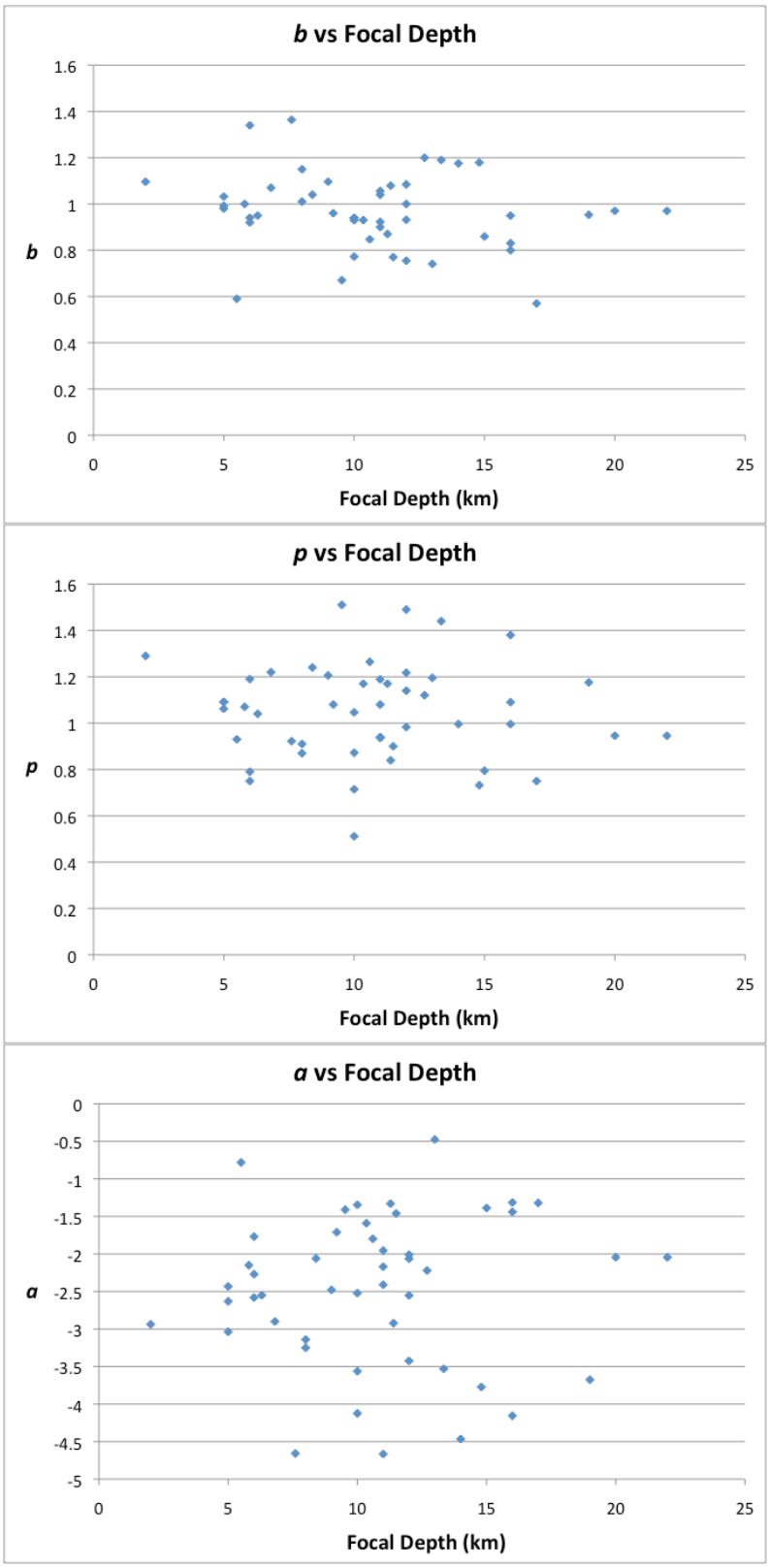

Figure 2. Correlations of the Omori-Law parameters (top) *b*, (middle) *p*, and (bottom) *a* with focal depth of the mainshock hypocenter.

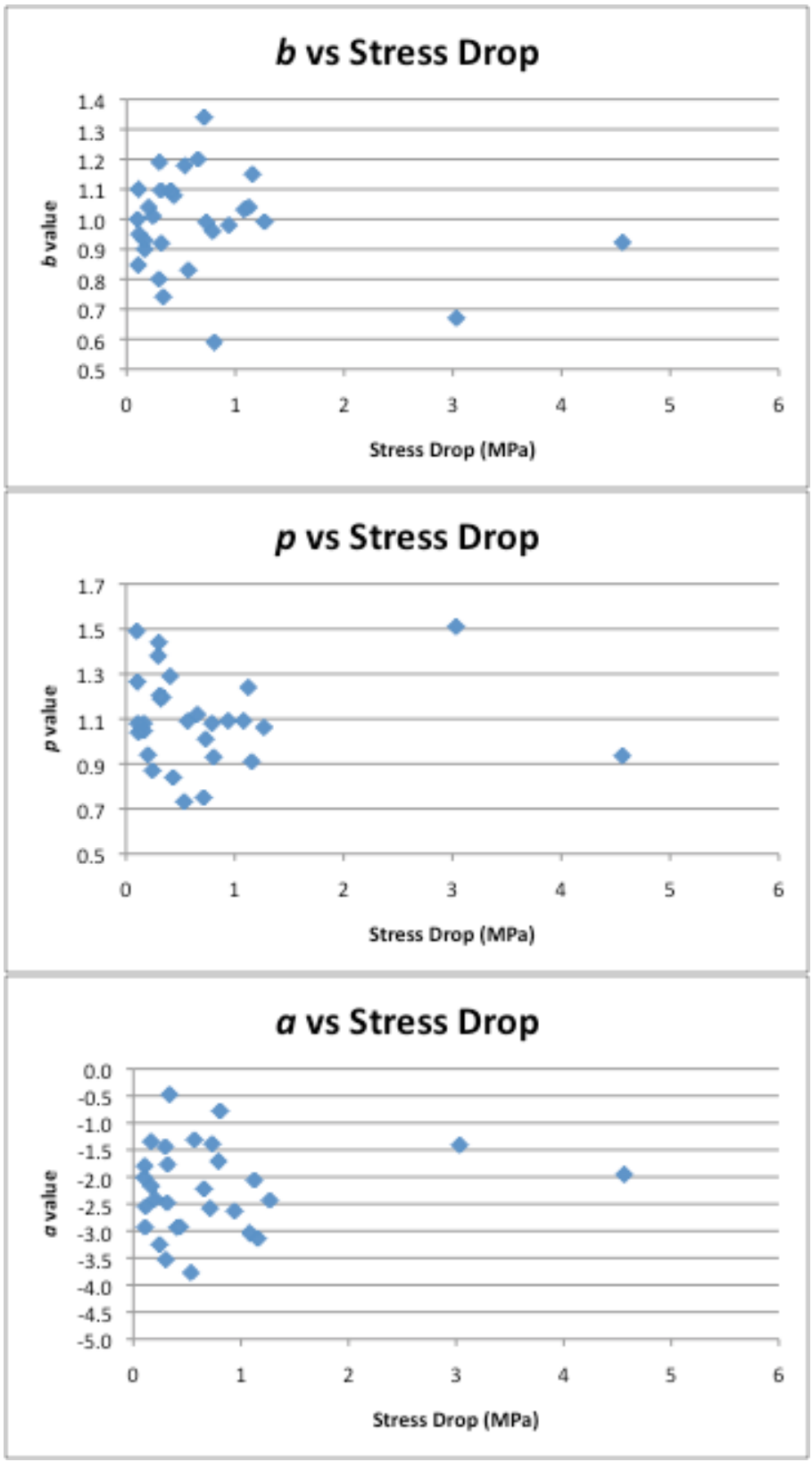

Figure 3. Correlations of the Omori-Law parameters (top) *b*, (middle) *p*, and (bottom) *a* with static stress drop of the mainshock.

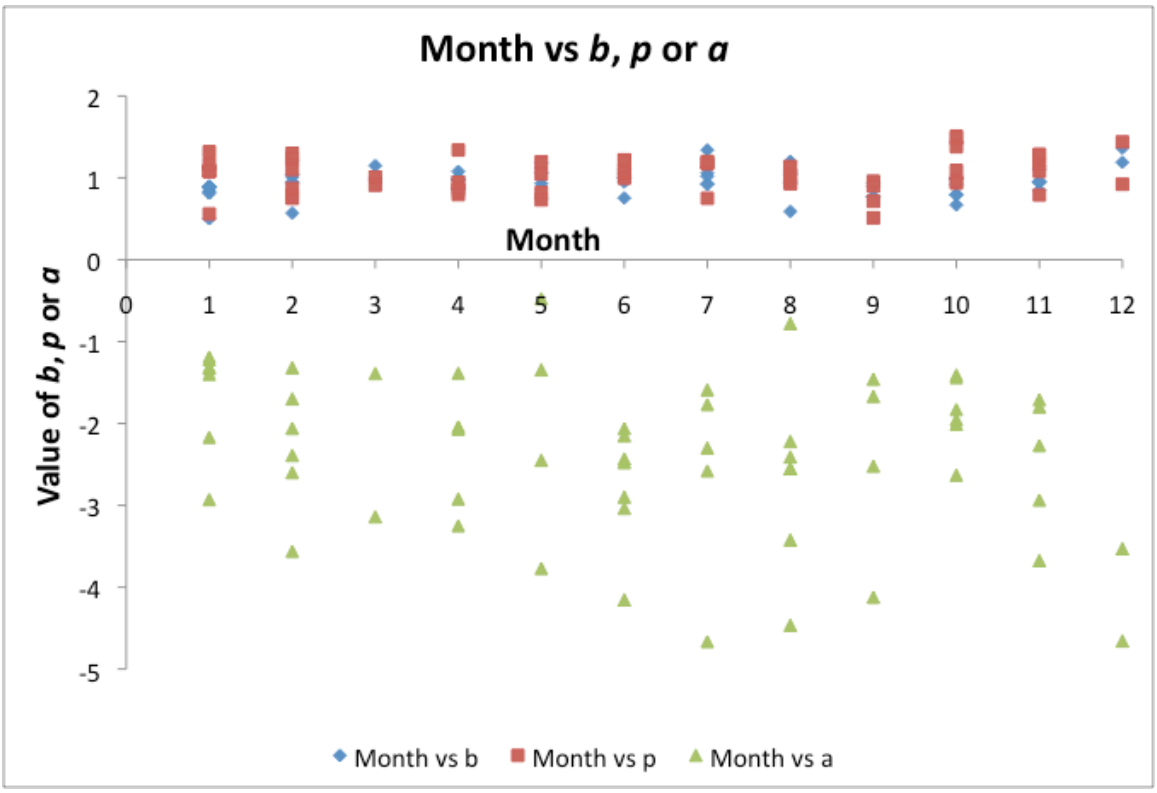

Figure 4. Correlations of the Omori-Law parameters *b*, *p*, and *a* with month of the year of the mainshock, with 1=January through 12=December.

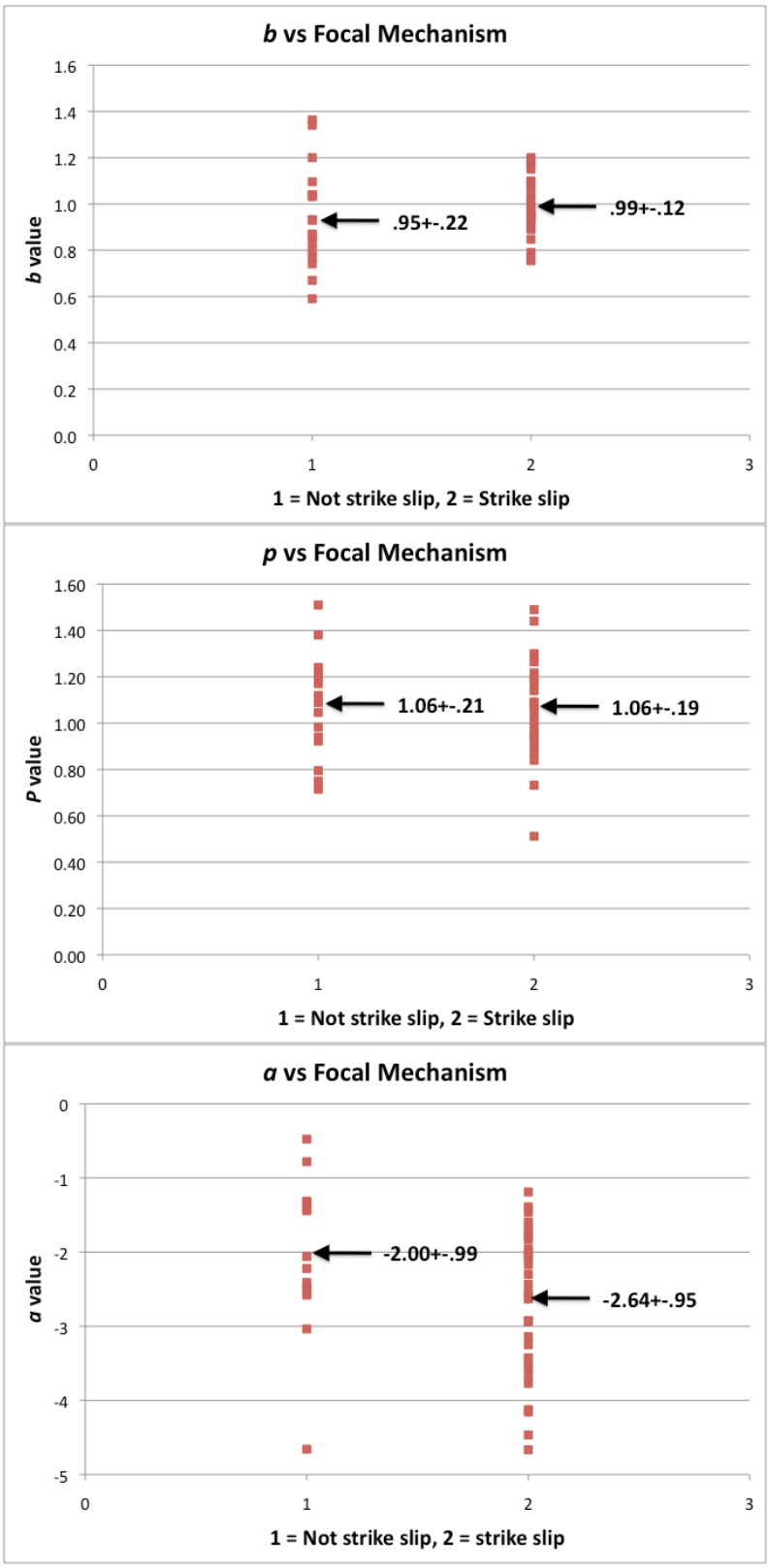

Figure 5. Correlations of the Omori-Law parameters (top) *b*, (middle) *p*, and (bottom) *a* with focal mechanism of the mainshock. For each set of data, an arrow indicates the mean and standard deviation.

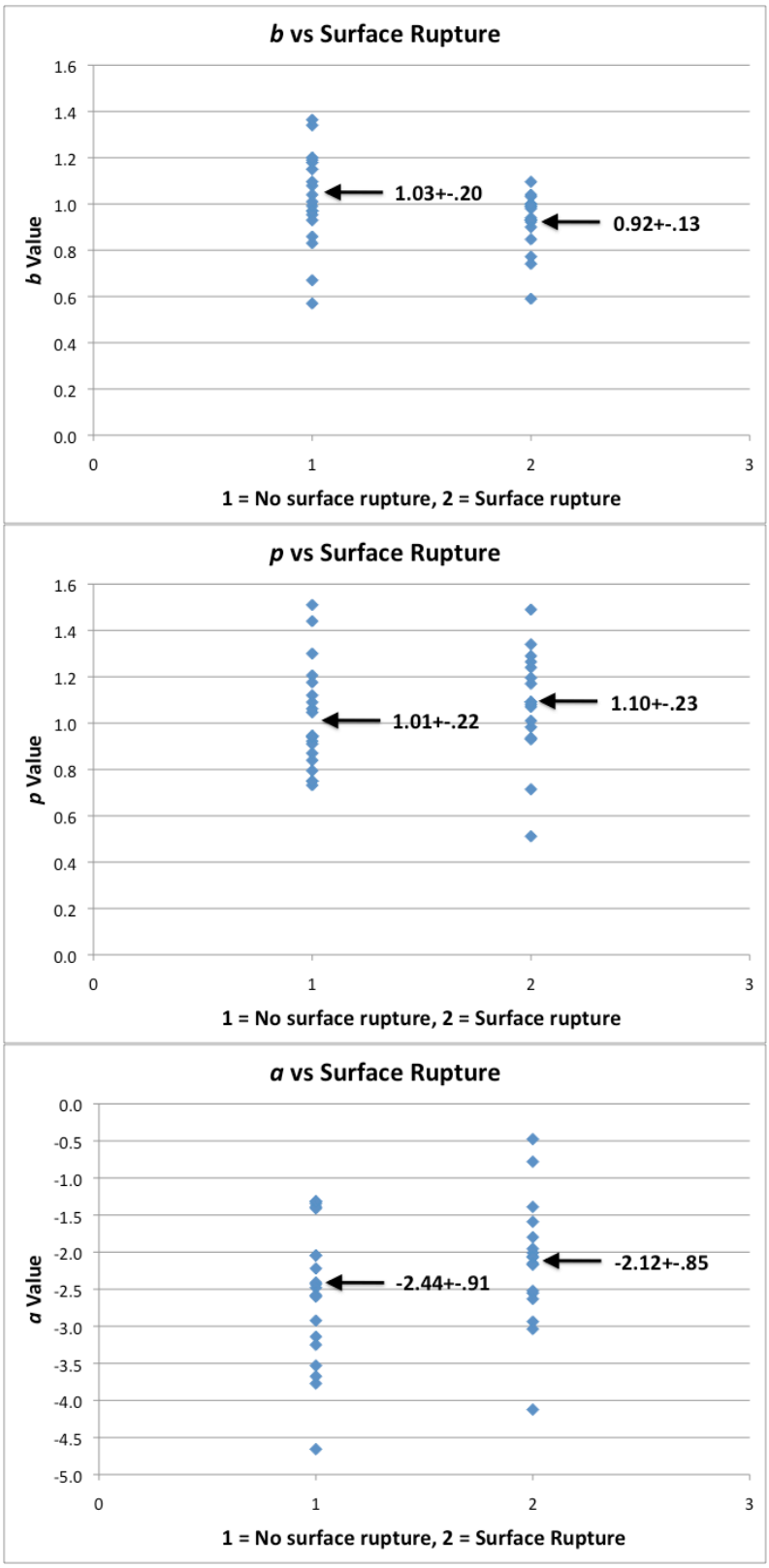

Figure 6. Correlations of the Omori-Law parameters (top) *b*, (middle) *p*, and (bottom) *a* with the presence or absence of surface faulting in the mainshock. For each set of data, an arrow indicates the mean and standard deviation.

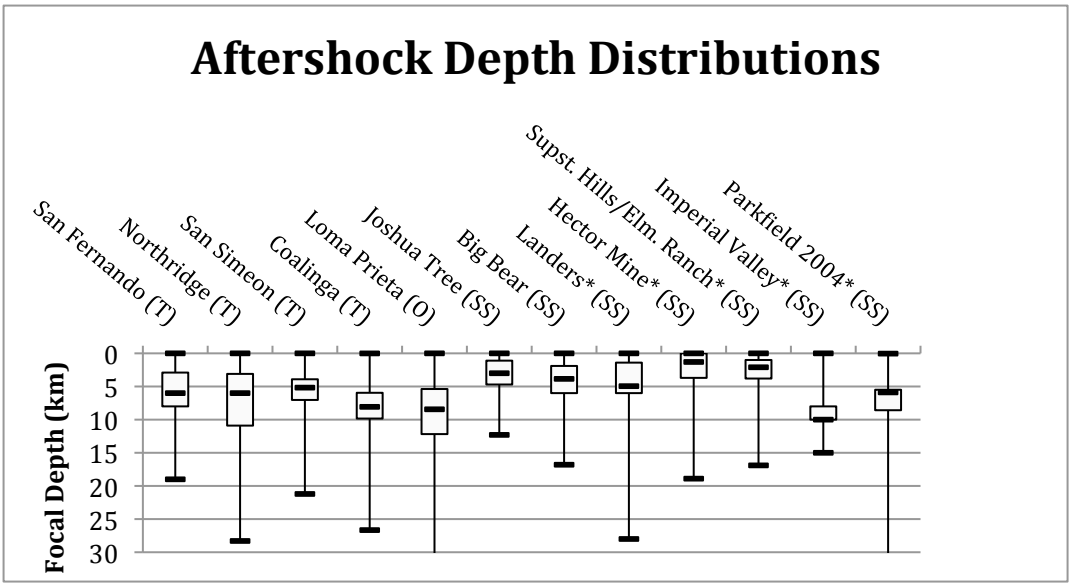

Figure 7. Box plots of the depth distributions of the aftershocks for several well-recorded mainshocks in California. The boxes indicate the depth range where 75% of the aftershocks took place. For each event, its focal mechanism is given at T=thrust, O=oblique slip or SS=strike-slip. Events with a * were those for which surface faulting occurred.